Inverse Analysis for Transient Thermal Load Identification and Application to Aerodynamic Heating on Atmospheric Reentry Capsule

Toshiya Nakamura (corresponding author)[1],

Yukihiro Kamimura[2], Hirotaka Igawa[1] and Yoshiki Morino[2]

[1] Structures Research Group, Japan Aerospace Exploration Agency

6-13-1 Osawa, Mitaka, Tokyo 181-0015 Japan

TEL: +81-50-3362-7014 FAX: +81-422-40-1434

Email: nakamt@chofu.jaxa.jp

[2] Dept. Applied Mechanics and Aerospace Eng., Waseda University

3-4-1 Okubo, Shinjuku, Tokyo 169-8555

Abstract

A transient inverse heat conduction analysis enables the identification of the unknown boundary heat flux from finite number of temperature data obtained e.g. in the high temperature structural tests or in the actual operation. Since the prediction of thermal load (heat flux) is difficult, the inverse analysis is expected to improve structural design of high temperature components. The present study develops a computational method of transient inverse heat conduction analysis. The developed code is applied to problems of a simple two-dimensional plate and of an atmospheric reentry capsule. Sequential function specification (SFS) method and Truncated Singular Value

Decomposition (TSVD) are employed to improve the stability of the inverse analysis. Effects of these regularization methods are numerically discussed.

Key Words: Transient Inverse Heat Conduction Analysis, Pseudo-inverse matrix, Sequential Function Specification, Truncated Singular Value Decomposition, Reentry Capsule

1 Introduction

Thermal analysis plays an important role in the structural design of high temperature components. However, prediction of thermal load (heat flux) is difficult due to physical complexity and uncertainties. The effect of uncertainties is significant in some cases and the probabilistic method is one of the promising approaches in the structural analysis [1]. One of the authors investigated the transient probabilistic thermal responses of a reentry capsule structure and its thermal reliability was assessed by Monte Carlo simulation [2].

Consequently it is useful if actual or operational thermal loads are identified from the temperature data obtained e.g. in the high temperature structural tests, high enthalpy wind tunnel tests or actual reentry flights. These identified load data may contribute to improving the load prediction method and hence the structural design [3], and to understanding the phenomena as well. As to the mechanical load identification, so-called operational load monitoring has a long history in many engineering fields including aerospace, but it is still attractive due to the significant progress of sensors and data pro-

cessing technologies today. The authors' group proposed a flexible method to reconstruct continuously distributed load (pressure) from finite number of strain data based on inverse elastic analysis [4].

The transient inverse heat conduction analysis is a way to estimate heat flux distribution and its history from finite number of temperature data. It has been studied by some researchers [5, 6, 7, 8, 9]. However, many of them are based on the finite difference method and can only be used for problems of simple geometry. Duda et al. developed a space marching method, which can be used to solve an inverse multidimensional heat conduction problem with complex-shaped bodies [8].

Generally, the transient inverse analysis is sensitive to the measurement error, measurement locations, and computational time step, but there have been few literatures on this issue. Ling and Atluri presented a method to analyze the error propagations in this problem [10].

In the present study, a computational method of transient inverse heat conduction analysis is developed to estimate the heat load from the temperature data. Our approach is based on the study by Duda [8]. In addition, a discrete representation of the boundary condition, which was proposed by the authors [4], is incorporated to allow for an approximation of the continuous heat load distribution with small number of degree of freedom (DOF). Applications to the simple two-dimensional problem and to the atmospheric reentry flight are demonstrated. The time-dependent heat flux distributions are reconstructed form the measured temperature data. The discussion will be focused on the computational stability and the regularization. The effects

of the Sequential Function Specification (SFS) and the Truncated Singular Value Decomposition (TSVD) will be numerically investigated.

It should be noted that another background of this study is the recent development of optical sensors. One of the authors has developed a long gauge FBG (Fiber Bragg Grating) sensor using OFDR (Optical Frequency Domain Reflectometry) technique. OFDR has a superior potential capable of measuring strains and temperatures at an arbitrary position along the fiber [11, 12]. The indication is that thousands of strain and temperature data will be acquired with less efforts, leading us to develop a load identification technique based on inverse analysis, because the inverse analysis requires a large amount of data to obtain a stable solution.

2 Procedure of Inverse Analysis

2.1 Fundamental Equations

The transient heat conduction equation within a body Ω is

$$\rho c\dot{T}(\boldsymbol{r},t) = \boldsymbol{\nabla}\cdot(\kappa\boldsymbol{\nabla}T(\boldsymbol{r},t)), \qquad \boldsymbol{r}\in\Omega, \tag{1}$$

where material properties c (specific heat), ρ (density), and κ (thermal conductivity) are assumed to be independent of temperature for simplicity, and the heat generation within the body is out of consideration.

We have an initial condition as

$$T(\boldsymbol{r},t_0) = T_0, \qquad \boldsymbol{r}\in\Omega. \tag{2}$$

The boundary conditions on the boundary $\partial\Omega = \partial\Omega_T \cup \partial\Omega_q \cup \partial\Omega_h$ are as

follows.

$$\left.\begin{array}{lll} \text{Specified temperature:} & T(\boldsymbol{r},t)=\bar{T}(\boldsymbol{r},t), & \boldsymbol{r}\in\partial\Omega_T \\ \text{Specified heat flux:} & \kappa\dfrac{\partial T}{\partial n}(\boldsymbol{r},t)=q(\boldsymbol{r},t), & \boldsymbol{r}\in\partial\Omega_q \\ \text{Convection:} & \kappa\dfrac{\partial T}{\partial n}(\boldsymbol{r},t)=h(T_\infty-T_{\Omega_h}), & \boldsymbol{r}\in\partial\Omega_h \end{array}\right\} \quad (3)$$

where n in Eq.(3) stands for the normal to the corresponding boundary. $\bar{T}, q, T_\infty, T_{\Omega_h}$ are the specified temperature, heat flux, environmental temperature, and structural temperature on $\partial\Omega_h$, respectively, and h is the convection coefficient.

The inverse problem is to identify the boundary condition as a function of $\boldsymbol{r}\in\partial\Omega$ and time from finite number of temperature data. The present study considers only the heat flux (Eq.$(3)_2$) for the boundary condition.

2.2 Discretization of Boundary Condition

In the authors' previous study of the inverse elastic analysis [4], the continuously distributed mechanical load (pressure distribution) was approximately represented by the combination of shape functions and nodal values. The unknown nodal values were identified from the finite number of strain data by the inverse operation. In the present study, we use the same method for the thermal boundary condition.

As shown in Fig.1, the spatially continuous heat flux distribution is approximated by Eq.(4).

$$q(\boldsymbol{r},t)=\sum_{i=1}^{N_q} N_i(\boldsymbol{r})q_i(t) \quad (4)$$

where q is the boundary heat flux and q_i is that at the i-th node. $N_i(\boldsymbol{r})$'s are the linear shape (interpolation) functions, and N_q is the number of nodes for the boundary condition approximation. The advantage of this method is

that the DOF of the inverse analysis N_q can be determined independently of the finite element model so that the stable solution is obtained.

2.3 Incremental Form

Ordinary finite element (FE) formulation yields the spatially discretized form of Eq.(1).

$$\boldsymbol{C}\dot{\boldsymbol{x}} + \boldsymbol{K}\boldsymbol{x} = \boldsymbol{R} \tag{5}$$

where $\boldsymbol{x}$ is a vector of nodal temperature of the FE model with the total number of nodes of N_x, that is,

$$\boldsymbol{x}(t) = (T_1(t), T_2(t), \cdots, T_{N_x}(t))^T. \tag{6}$$

$\boldsymbol{C}$ and $\boldsymbol{K}$ are the capacitance matrix and the conductance matrix, respectively, and $\boldsymbol{R}$ is the thermal load vector [13].

We rewrite Eq.(5) in the form of Eq.(7) [8].

$$\dot{\boldsymbol{x}} = \boldsymbol{F}\boldsymbol{x} + \boldsymbol{G}\boldsymbol{q} \tag{7}$$

where $\boldsymbol{q}$ is a vector of the nodal values of the boundary heat flux in the form of Eq.(4), thus,

$$\boldsymbol{q}(t) = \big(q_1(t), q_2(t), \cdots, q_{N_q}(t)\big)^T. \tag{8}$$

The initial condition is

$$\boldsymbol{x}(t_0) = (T_1(t_0), T_2(t_0), \cdots, T_{N_x}(t_0))^T. \tag{9}$$

The dimensions of the coefficient matrices $\boldsymbol{F}$ and $\boldsymbol{G}$ are $N_x \times N_x$ and $N_x \times N_q$, respectively.

The incremental form of Eq.(7) can be written as [8]

$$\boldsymbol{x}((k+1)\Delta t) = \boldsymbol{A}\boldsymbol{x}(k\Delta t) + \boldsymbol{B}\boldsymbol{q}(k\Delta t) \tag{10}$$

where $N_x \times N_x$ matrix $\boldsymbol{A}$ and $N_x \times N_q$ matrix $\boldsymbol{B}$ depend on Δt.[1]

Using the time step k for the time t, we have the following incremental form.

$$\begin{cases} \boldsymbol{x}(k+1) = \boldsymbol{A}\boldsymbol{x}(k) + \boldsymbol{B}\boldsymbol{q}(k) \\ \boldsymbol{y}(k) = \boldsymbol{M}\boldsymbol{x}(k) \end{cases} \tag{11}$$

where $\boldsymbol{y}(k)$ is a vector of temperature data at time step k, whose elements are

$$\boldsymbol{y}(k) = \left(T_1^m(k), T_2^m(k), \cdots, T_{N_y}^m(k)\right)^T. \tag{12}$$

$N_y \times N_x$ matrix $\boldsymbol{M}$ extracts the temperature data at the measurement locations from $\boldsymbol{x}$ (the full set of temperature at the entire nodes of FE model).

2.4 Solution

In solving Eq.(11) for $\boldsymbol{q}(k)$, $\boldsymbol{x}(k+1)$ is not known at the time step k, but $\boldsymbol{y}(k+1)$ is already available because it is the measured data. Then by substituting $\boldsymbol{y}(k+1)$ for $\boldsymbol{x}(k+1)$, we have

$$\tilde{\boldsymbol{q}}(k) \;=\; (\boldsymbol{M}\boldsymbol{B})^+ \left[\boldsymbol{y}(k+1) - \boldsymbol{M}\boldsymbol{A}\tilde{\boldsymbol{x}}(k)\right] \tag{13}$$

[1] Mathematical representations of the matrices $\boldsymbol{A}$ and $\boldsymbol{B}$ are as follows[8].

$$\boldsymbol{A} = \boldsymbol{I} + \sum_{n=1}^{\infty} \frac{1}{n!}(\boldsymbol{F}\Delta t)^n, \quad \boldsymbol{B} = \left\{\boldsymbol{I} + \sum_{n=1}^{\infty} \frac{1}{(n+1)!}(\boldsymbol{F}\Delta t)^n\right\} \boldsymbol{G}\Delta t$$

We determined these coefficient matrices numerically through the ordinary finite element formulation with fixed Δt. Equation(10) is integrated for Δt (one step) by FEM with $\boldsymbol{x}(0) = (1, 0, \cdots, 0)^T$ and $\boldsymbol{q}(0) = \boldsymbol{0}$. The result is $\boldsymbol{x}(\Delta t) = (A_{11}, A_{12}, \cdots, A_{1N_x})^T$. This process is repeated to determine all components of $\boldsymbol{A}$ and $\boldsymbol{B}$.

where $\tilde{\boldsymbol{q}}(k)$ is the vector of the estimated boundary heat flux, and

$$\tilde{\boldsymbol{x}}(k) \quad = \quad \boldsymbol{A}\tilde{\boldsymbol{x}}(k-1) + \boldsymbol{B}\tilde{\boldsymbol{q}}(k-1) \tag{14}$$

is the temperature calculated as a response to the boundary condition estimated at the previous steps. $N_q \times N_y$ matrix $(\boldsymbol{MB})^+$ is the pseudo-inverse matrix of $\boldsymbol{MB}$.

3 Regularization

Usually, the transient inverse heat conduction problem is ill-posed. The computational stability is strongly sensitive to the measurement error. Thus the regularization is inevitable to stabilize the numerical calculation. In this study, the Sequential Function Specification (SFS) method [5, 6, 14] and the Truncated Singular Value Decomposition (TSVD) are employed that are briefly explained in the following subsections. The SFS will be used in the two-dimensional case, and both SFS and TSVD will be employed in the analysis of a reentry capsule.

3.1 Sequential Function Specification (SFS)

Sequential Function Specification (SFS) method or Beck's method adds stability by considering N_F future time steps at step k and making the temporary (but incorrect) assumption that

$$\boldsymbol{q}(k) = \boldsymbol{q}(k+1) = \cdots = \boldsymbol{q}(k+N_F). \tag{15}$$

With Eq.(15), the state equation for the future time steps $r(= 1, \cdots, N_F)$

is consequently written as

$$\begin{cases} \boldsymbol{x}(k+r) = \boldsymbol{A}^r \boldsymbol{x}(k) + \sum_{j=1}^{r} \boldsymbol{A}^{r-j} \boldsymbol{B} \boldsymbol{q}(k) \\ \boldsymbol{y}(k+r) = \boldsymbol{M} \boldsymbol{x}(k+r) \end{cases} \tag{16}$$

Finally we have the following equation

$$\boldsymbol{Y}(k+1) = \boldsymbol{P}\boldsymbol{x}(k) + \boldsymbol{D}\boldsymbol{q}(k) \tag{17}$$

where

$$\boldsymbol{Y}(k+1) = (\boldsymbol{y}(k+1), \boldsymbol{y}(k+2), \cdots, \boldsymbol{y}(k+N_F))^T \tag{18}$$

$$\boldsymbol{P} = \left(\boldsymbol{MA}, \boldsymbol{MA}^2, \cdots, \boldsymbol{MA}^{N_F}\right)^T \tag{19}$$

$$\boldsymbol{D} = \left(\boldsymbol{MAB}, \boldsymbol{M}\sum_{j=1}^{2} \boldsymbol{A}^{2-j}\boldsymbol{B}, \cdots, \boldsymbol{M}\sum_{j=1}^{N_F} \boldsymbol{A}^{N_F-j}\boldsymbol{B}\right)^T \tag{20}$$

Equation (17) is solved to estimate the unknown heat flux $\tilde{\boldsymbol{q}}$ as

$$\tilde{\boldsymbol{q}}(k) = \boldsymbol{D}^+ \left[\boldsymbol{Y}(k+1) - \boldsymbol{P}\tilde{\boldsymbol{x}}(k)\right] \tag{21}$$

where $N_q \times N_F N_y$ matrix $\boldsymbol{D}^+$ is the pseudo-inverse matrix of $\boldsymbol{D}$.

3.2 Truncated Singular Value Decomposition (TSVD)

The singular value decomposition (SVD) of the matrix $\boldsymbol{D}$ is written as

$$\boldsymbol{D} = \sum_{j=1}^{R} \lambda_j \boldsymbol{w}_j \boldsymbol{v}_j^T \tag{22}$$

where R and λ_j $(j = 1, \cdots, R)$ are the rank and the non-zero singular values of $\boldsymbol{D}$ $(1 \leq R \leq \min(N_F N_y, N_q))$, and $\boldsymbol{v}_j$ and $\boldsymbol{w}_j$ are the normalized eigen vectors of the square matrices $\boldsymbol{D}^T\boldsymbol{D}$ and $\boldsymbol{D}\boldsymbol{D}^T$, respectively. This SVD yields the pseudo-inverse matrix of Moore-Penrose $\boldsymbol{D}^+$ as[15]

$$\boldsymbol{D}^+ = \sum_{j=1}^{R} \frac{1}{\lambda_j} \boldsymbol{v}_j \boldsymbol{w}_j^T \tag{23}$$

Equations (21) and (23) indicate that small singular values make the calculation quite sensitive to the measurement error, and as a consequence the inverse analysis may become unstable. A representative method to overcome this difficulty is to reduce the rank of the matrix by truncating the small singular values (TSVD).

4 Two-dimensional Problem

Figure 2 shows the two-dimensional problem. We consider a square plate ABCD whose side length L, with the following boundary condition.

$$q(x,y,t) = \begin{cases} \hat{q}(t), & \text{on AA'} \\ -\hat{q}(t), & \text{on CC'} \\ 0, & \text{on other boundary} \end{cases} \tag{24}$$

and

$$\hat{q}(t) = \begin{cases} 0, & 0 \le t < t_0 \\ \dfrac{Q_1}{t_1 - t_0}(t - t_0), & t_0 \le t < t_1 \\ Q_1, & t_1 \le t < t_2 \\ Q_2, & t_2 \le t < t_3 \end{cases} \tag{25}$$

where the coordinates of A, A', C, C' are A$(0,0)$, A'$(L/2,0)$, C(L,L), C'$(L/2,L)$, respectively, and $L = 0.5$m, $t_0 = 50$sec., $t_1 = 100$sec., $t_2 = 300$sec., $t_3 = 450$sec., $Q_1 = 50\text{kW/m}^2$, $Q_2 = 100\text{kW/m}^2$. The heat flux $\hat{q}(t)$ of Eq.(25) is shown in Fig.2(b) (bold line).

First, the direct finite element analysis was conducted. Then the boundary heat flux was inversely estimated using the temperature data at all nodes on the boundary ABCD obtained by the direct FE analysis. The artificial measurement error was considered by adding small random deviation ΔT to the nodal temperature at each time step. The distribution of ΔT is Gaussian

where the mean value is zero and the standard deviation is 2 °C.

In the inverse analysis, Eq.(4) is used to approximate the unknown spatial distribution of q with the DOF N_q=80 (20 for each side). The conditions of the analysis are summarized in Table 1.

Figures 2(b),(c) and (d) show the inverse analysis results. It is found that the solution is unstable due to the measurement error without regularization and that the SFS effectively stabilize the calculation. It is noted that the SFS parameter of $N_F = 20$ was empirically determined.

5 Application to Reentry Capsule

5.1 Piggyback Atmospheric Reentry Technology Testbed (PARTT)

Japan Aerospace Exploration Agency (JAXA) conducted a conceptual study of a reentry testbed "PARTT" (Piggyback Atmospheric Reentry Technology Testbed). The PARTT was planned to be delivered into orbit as a "piggyback" using surplus payload capacity of a launch vehicle.

Referring to the standard piggyback payload of the Japanese H-IIA launch vehicle, the weight and the diameter of the PARTT reentry module were designed to be 40kg and 0.7m, respectively. The materials and dimensions of the reentry module are summarized in Table 2 and Fig. 3. Details were reported by Fujii et al. in [16, 17].

5.2 Heat Flux

The heat flux $q_0(t)$ at the stagnation point of a 0.7m diameter sphere was calculated along the nominal reentry trajectory using the Fay-Riddell equa-

tion as shown in Fig.4(a). This $q_0(t)$ will be used as a reference heat flux history.

The design concept of the PARTT heat shield is that the emission from the back surface of the shell suppresses temperature increase. An elliptic cross-section was selected for the sake of this.

The heat flux distribution on the shell at the time when $q_0(t)$ in Fig. 4(a) reaches its peak value was calculated by CFD (computational fluid dynamics) assuming an ideal gas and axisymmetry (zero angle of attack). The result is shown in Fig. 4(b) in terms of the distribution function $\phi(r/r_0)$ which is a ratio of the heat flux distribution $q(r/r_0)$ on the shell to the highest reference heat flux where r_0 is the radius of the shell. The CFD analysis showed that the aerodynamic heat flux on the shell takes the highest value close to the edge. By adopting an elliptical shape, the maximum heat flux is reduced to about 70% of that of a sphere.

For simplicity, the distribution $\phi(r/r_0)$ was assumed not to change during the reentry flight. Then the nominal aerodynamic heat flux is calculated by

$$q_n(r,t) = \phi\left(\frac{r}{r_0}\right) q_0(t) \tag{26}$$

on the front surface of heat shield shell.

The heat transfer between the hot structure and the cold air around the capsule may be significant at low altitude but is ignored for simplicity.

5.3 Direct Analysis

The temperature data for the inverse analysis was prepared by the direct FE analysis with the heat flux of Eq.(26). The FE model is composed of 473

four-nodes axisymmetric elements with 590 nodes as shown in Fig.5.

Figure 6 shows the temperature histories at several points obtained by the direct FE analysis. The highest temperature takes place near the edge of the heat shield shell. The high temperature at G is attributed to the emission from the back surface of the heat shield. Corresponding to $q_0(t)$ in Fig.4(a), the temperatures of the shell and at G decrease after 200 sec. due to the heat dissipation into the backward structure and emission. On the other hand, the temperatures at D and F increase after 150 sec. This is attributed to the radiative and conductive heat coming from the high temperature heat shield.

5.4 Inverse Analysis

We consider the net heat flux q_{net} which includes the aerodynamic heat flux on the front surface of the heat shield, the emission into the space and that from different part of the structure. This is because the present method does not distinguish these different heat sources. The inverse problem in this study is to identify the distribution and history of q_{net} not only on the shell surface but on the entire outer surface.

Locations of the temperature measurement are the all nodes of the FE model on the bold lines of Fig.5. The total number of measurement points is N_y=187. For the approximation of the heat flux distribution, we have N_q=55 in Eq.(4).

The measurement error was artificially added to the temperature data. This noise follows the Gaussian distribution, whose mean and standard deviation are 0 and 20 °C, respectively.

5.5 Results

It was found again that the analysis is unstable due to the measurement error without regularization. Then SFS and TSVD are employed. The SFS parameter $N_F = 20$ was empirically determined for the present application and assumed artificial measurement data. The rank of the matrix $\boldsymbol{D}$ was reduced from 55 (full rank) to 46 by TSVD. The effects of them will be discussed in the next subsection.

Figures 7(a-d) show the history of the net heat flux at points A, B, C, and D in Fig.3. Good agreements are found between the inverse analysis results and the pre-assumed heat flux histories. Negative heat flux in Figs. 7(a-c) are attributed to the emission from the heat shield shell. The emission from the back surface of the heat shield reaches the backward structure, resulting in the increase of the heat flux in Fig.7(d) after 150sec.

5.6 Effects of Regularization

Figure 8 shows the results at point C with and without TSVD where the parameter of SFS N_F=20. When the rank of the matrix $\boldsymbol{D}$ is not reduced, the estimation fails. On the other hand, TSVD significantly improves the estimation.

The singular values (SV) of the matrix $\boldsymbol{D}$ of the present system is shown in Fig.9 for different N_F. It shows that the larger N_F results in the larger SV, hence the robustness is improved. The effect of SFS is shown in Figs.10(a-c) for $N_F = 10$, 20 and 30, respectively. In these calculations, the rank of matrix $\boldsymbol{D}$ was truncated to be 46. Corresponding to the observation in Fig.9, it is

found that larger N_F results in less dispersion of the solution. But if we take too many N_F, the estimation goes ahead of the target value.

6 Conclusion

A computational method of the transient inverse heat conduction analysis was developed based on the discrete state equation formulation. The developed method has been applied to the heat load identification problems of the simple two-dimensional plate and the reentry capsule. Time-varying heat flux distributions were reconstructed from the measured temperature data.

Numerical simulation showed that good estimation can be obtained by using regularization techniques. Within the present study, a combination of TSVD and SFS improves the estimation with measurement error.

It should be noted that the criterion for the selection of measurement points is not clear within the present study. Considering the discussion on the regularization, one can select the points so that there are as many singular values as possible beyond the criterion. But at this time, we do not have mathematically rigorous procedure to determine the proper values of the regularization parameters. This is of practical importance in the actual application to design the location of the sensors and to suppress the adverse effect of the measurement error or noise. Finally, an extension to the nonlinear problem with temperature-dependent material properties is also an important future issue.

References

[1] D. Xiu and G. E. Karniadakis, "A New Stochastic Approach to Transient Heat Conduction Modeling with Uncertainty", International Journal of Heat and Mass Transfer 46, 2003, pp. 4681-4693.

[2] T. Nakamura and K. Fujii, "Probabilistic Transient Thermal Analysis of an Atmospheric Reentry Vehicle Structure", Aerospace Science and Technology 10, 2006, pp. 346-354.

[3] O. M. Alifanov, "Mathematical and Experimental simulation in aerospace system verification", Acta Astronautica, 41, 1997, pp. 43-52.

[4] T. Nakamura, H. Igawa and A. Kanda, "Inverse Identification of Continuously Distributed Loads Using Strain Data", Aerospace Science and Technology 23, 2012, pp.75-84.

[5] J. V. Beck, B. Blackwell and C. R. St. Clair, Jr., "Inverse Heat Conduction: Ill-Posed Problems", Wiley-Interscience, New York, 1985.

[6] J. V. Beck, "Inverse Problems," in Handbook of Numerical Heat Transfer, Wiley, 1988, pp. 787-834.

[7] J. Taler and P. Duda, "Solving Direct and Inverse Heat Conduction Problems", Springer, 2006.

[8] P. Duda, "Solution of Multidimensional Inverse Heat Conduction Problem", Heat and Mass Transfer 40, 2003, pp. 115-122.

[9] P. Duda, J. Taler and E. Roos, "Inverse Method for Temperature and Stress Monitoring in Complex-Shaped Bodies", Nuclear Engineering and Design 227, 2004, pp. 331-347.

[10] X. Ling and S.N. Atluri, "Stability Analysis for Inverse Heat Conduction Problems", Computer Modeling in Engineering and Sciences, vol.13, No.3 (2006), pp.219-228.

[11] H. Igawa, H. Murayama, T. Kasai,I. Yamaguchi, K. Kageyama, and K. Ohta, "Measurements of Strain Distributions with a Long Gauge FBG Sensor using Optical Frequency Domain Reflectometry", Proc. of SPIE, Vol.5855, 2005, pp.547-550.

[12] H. Igawa, K. Ohta, T. Kasai, I. Yamaguchi, H. Murayama and K. Kageyama, "Distributed Measurements with a Long Gauge FBG Sensor Using Optical Frequency Domain Reflectometry (1st Report, System Investigation Using Optical Simulation Model)", Journal of Solid Mechanics and Materials Engineering, 2(9), 2008, pp.1242-1252.

[13] E.A. Thornton, "Thermal Structures for Aerospace Applications", AIAA Education Series, 1996, pp.286-290.

[14] J. V. Beck, "Surface Heat Flux Determination Using an Integral Method", Nuclear Engineering and Design 7, 1968, pp. 170-178.

[15] G.H. Golub and C.F. Van Loan, §5.5.4. "The pseudo-inverse", in Matrix Computations, 3rd edition, The Johns Hopkins University Press, pp. 257-258, 1996.

[16] K. Fujii, T. Tsuchiya, T. Kai, T. Ito, S. Watanabe, T. Nakamura, S. Ishimoto, H. Kawato, K. Nishiwaki and M. Shirouzu, "Concepts of Reentry Technology Experimental Vehicles", AIAA 2002-5264.

[17] K. Fujii, T. Nakamura, H. Kawato and S. Watanabe, "Concepts and Studies of Flight Experiment Vehicles for Reusable Space Transportation System", AIAA 2003-6984.

List of Tables and Figures

Tables

Table 1 Conditions of Two Dimensional Analysis
Table 2 Specifications of Reentry Module

Figures

Figure 1 Discrete Modeling of Boundary Condition
Figure 2 Inverse Analysis of 2D Plate
Figure 3 Reentry Module Structure
Figure 4 Aerodynamic Heat Flux
Figure 5 Axisymmetric FE Model and Measurement Locations (Nodes on the Bold Lines)
Figure 6 Inverse Analysis Results
Figure 7 Temperature of PARTT Structure (Direct FE Analysis)
Figure 8 Effect of TSVD at C
Figure 9 Singular Values of the Matrix $\boldsymbol{D}$
Figure 10 Result at C with Sequential Function Specification

Table 1: Conditions of Two Dimensional Analysis

Material	Titanium
Density	4507 kg/m^3
Specific Heat	520 J/kgK
Thermal Conductivity	21.9 W/mK
Initial Temperature T_0	0 °C, Uniform
Time Increment ΔT	1 sec.
Number of Nodes	2601
Number of Nodes on Boundary	200 (50 on each side)
Measurement Error	Gaussian
Mean	0 °C
Standard Deviation	2 °C
DOF of Inverse Analysis N_q	80
SFS Parameter N_F	20

Table 2: Specifications of Reentry Module

	Material	Dimensions (mm)
Heat Shield Shell	C/C Composite	Diameter 700, Thickness 10
Support	C/C Composite	Diameter 460, Height 80
Insulator	Macelite	Outer D. 460, Thickness 10
Inner Insulator	Rigid Ceramic Tile	Diameter 440, Thickness 50
Body	Al Alloy	Diameter 460, Thickness 10

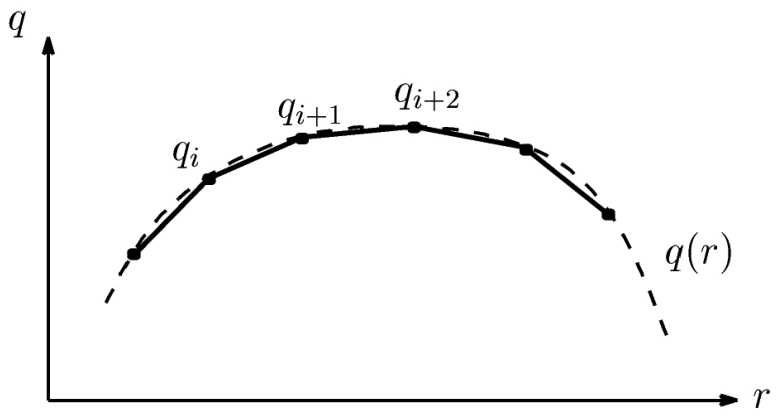

Figure 1: Discrete Modeling of Boundary Condition

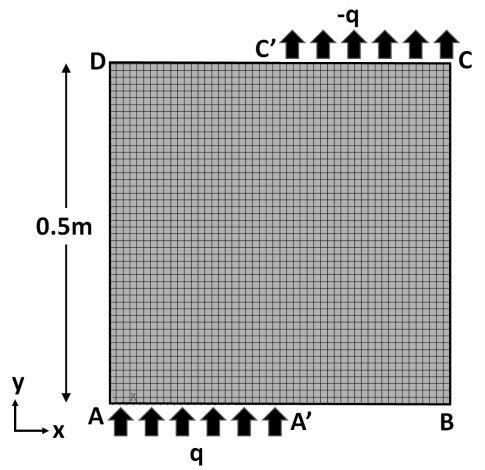

(a) 2D Model

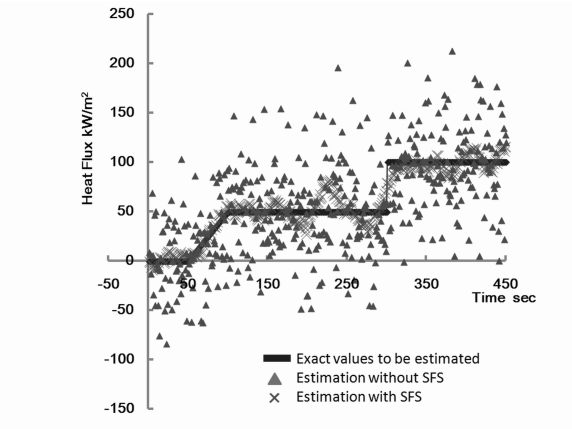

(b) History of Heat Flux $\hat{q}(t)$

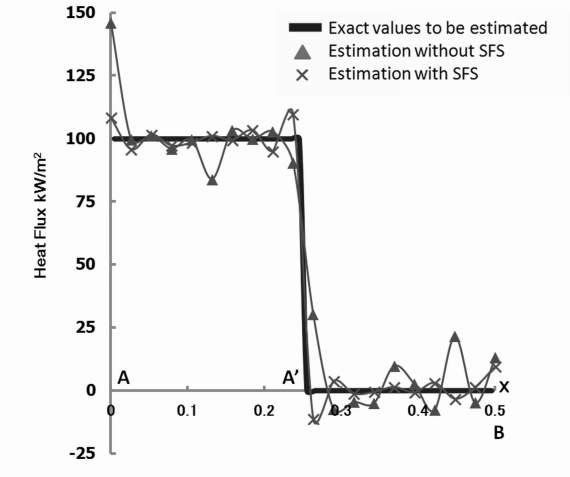

(c) Heat Flux Distribution on AB at 400sec.

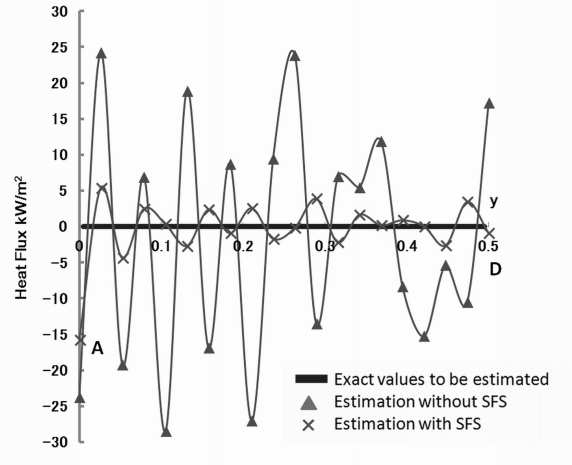

(d) Heat Flux Distribution on AD at 400sec.

Figure 2: Inverse Analysis of 2D Plate

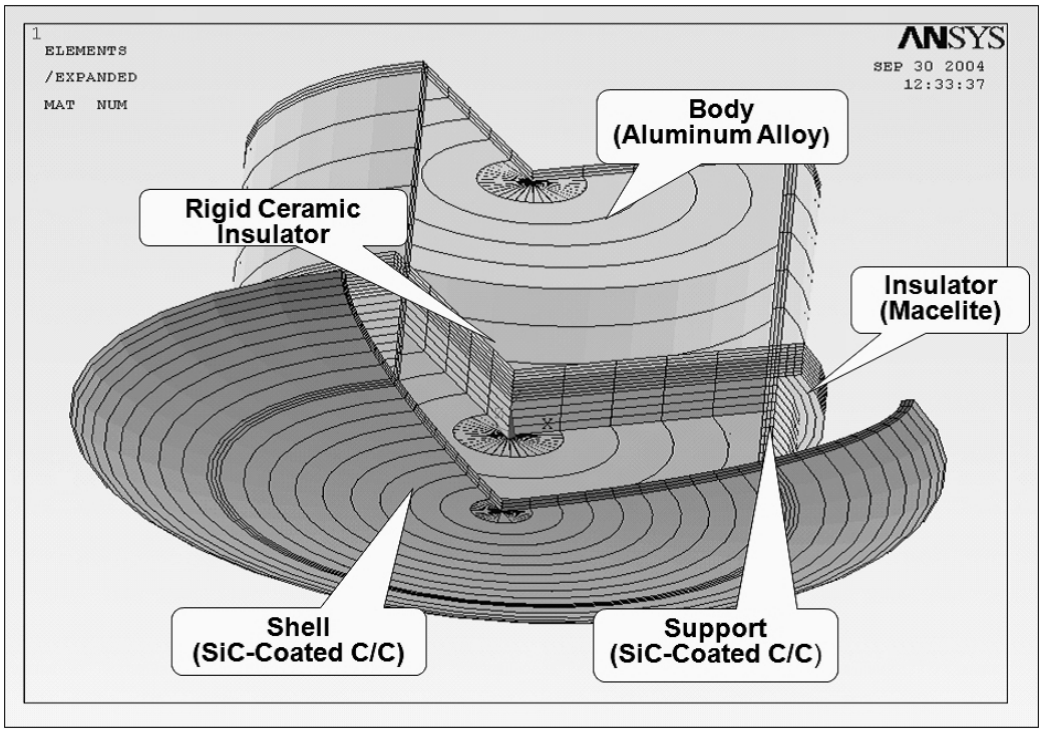

Figure 3: Reentry Module Structure

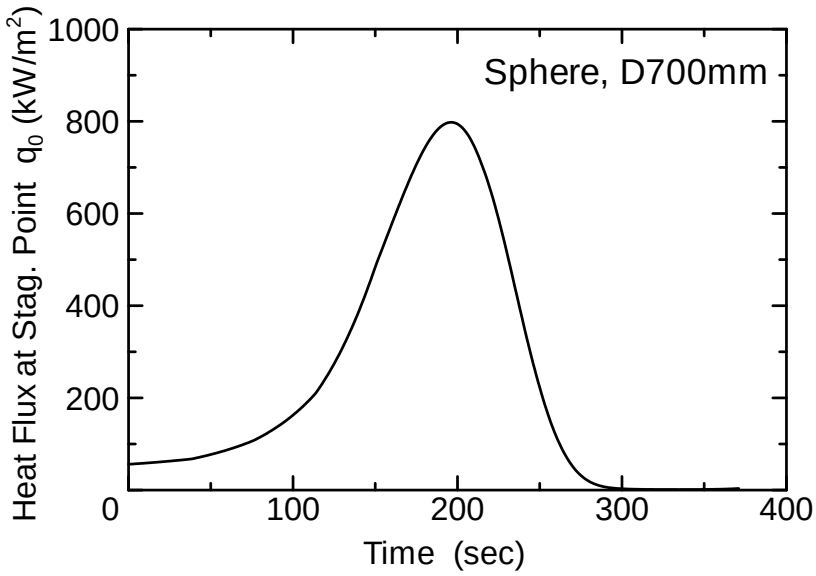

(a) Reference Heat Flux History $q_0(t)$

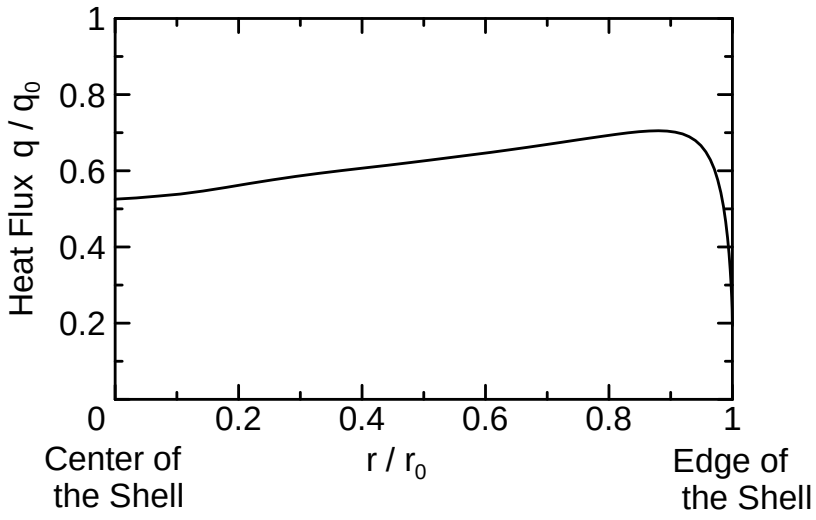

(b) Heat Flux Distribution on the Shell

Figure 4: Aerodynamic Heat Flux

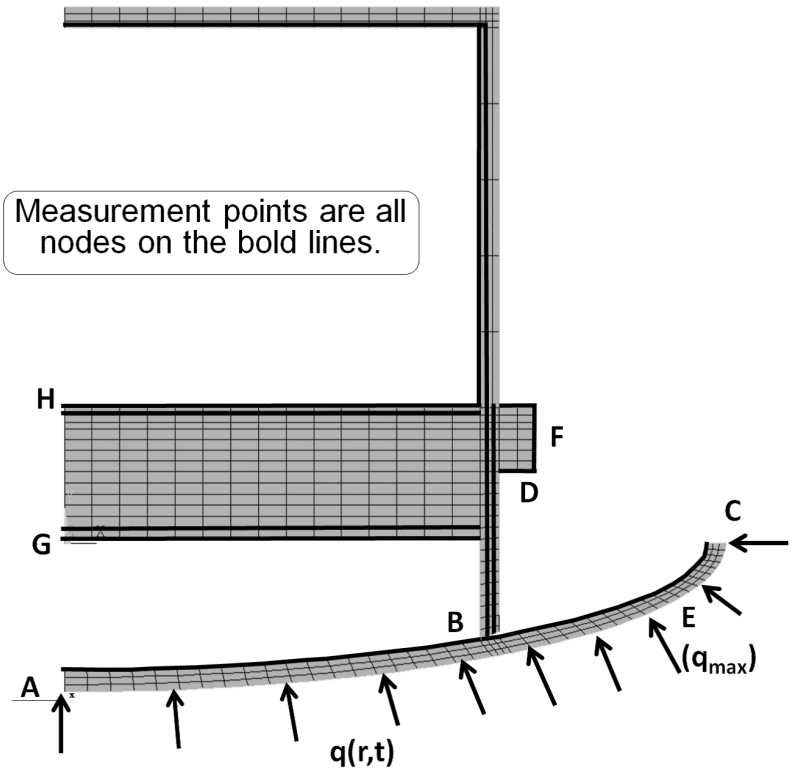

Figure 5: Axisymmetric FE Model and Measurement Locations (Nodes on the Bold Lines)

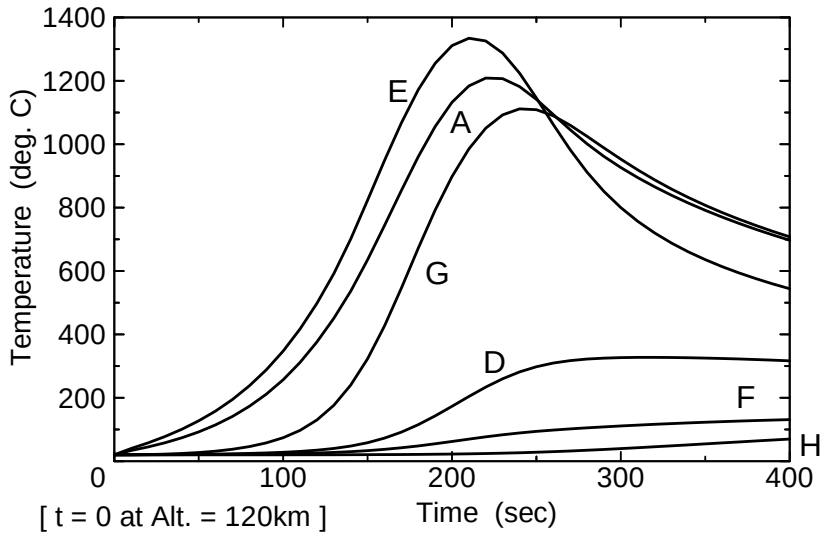

Figure 6: Temperature of PARTT Structure (Direct FE Analysis)

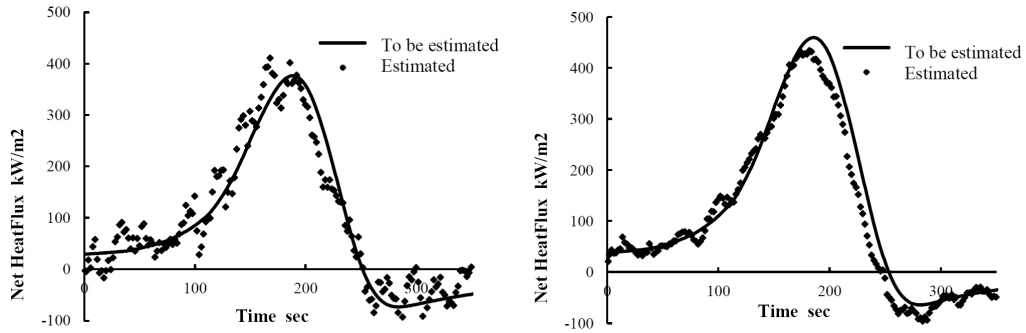

(a) q_{net} at A

(b) q_{net} at B

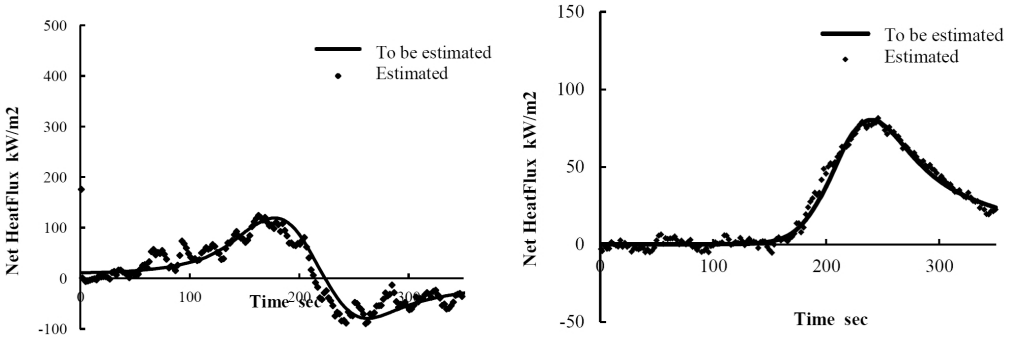

(c) q_{net} at C

(d) q_{net} at D

Figure 7: Inverse Analysis Results

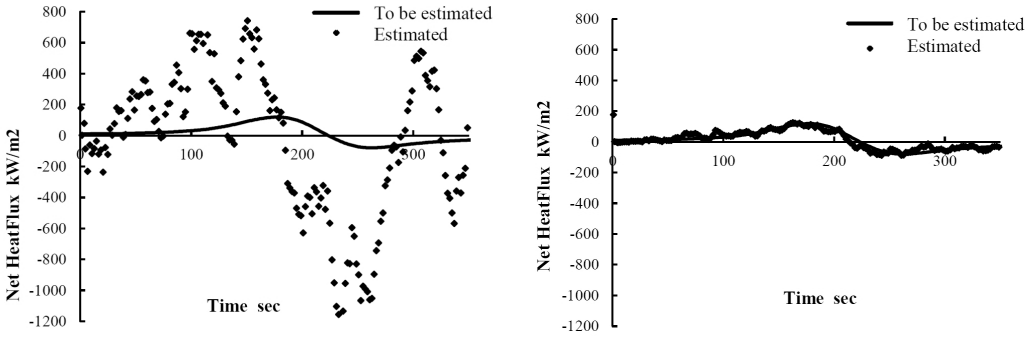

(a) Without TSVD

(b) With TSVD

Figure 8: Effect of TSVD at C

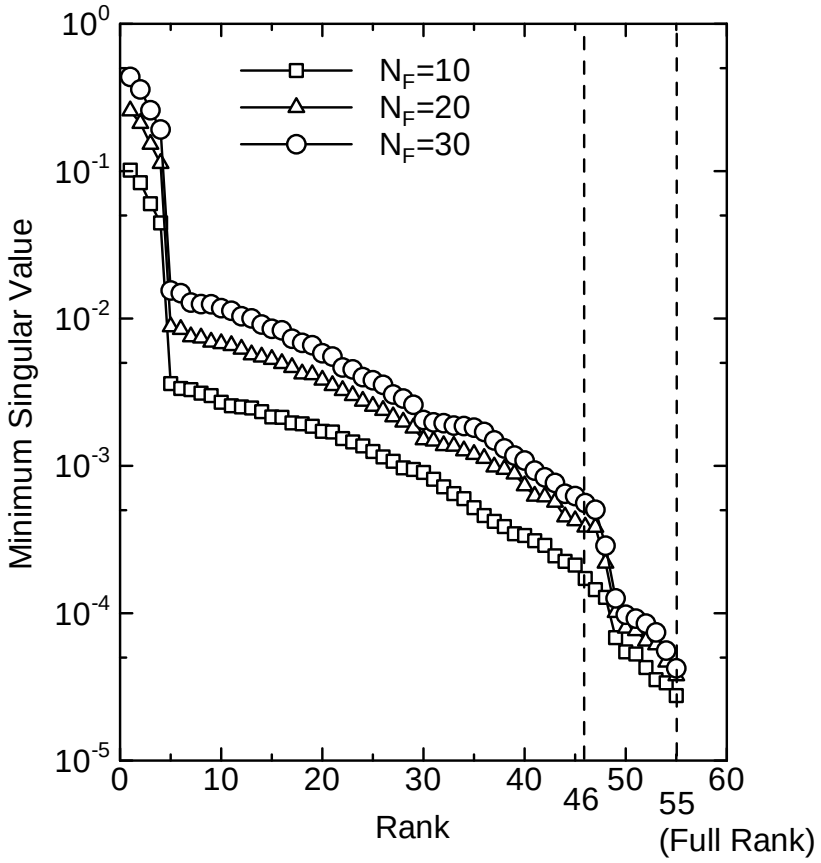

Figure 9: Singular Values of the Matrix $\boldsymbol{D}$

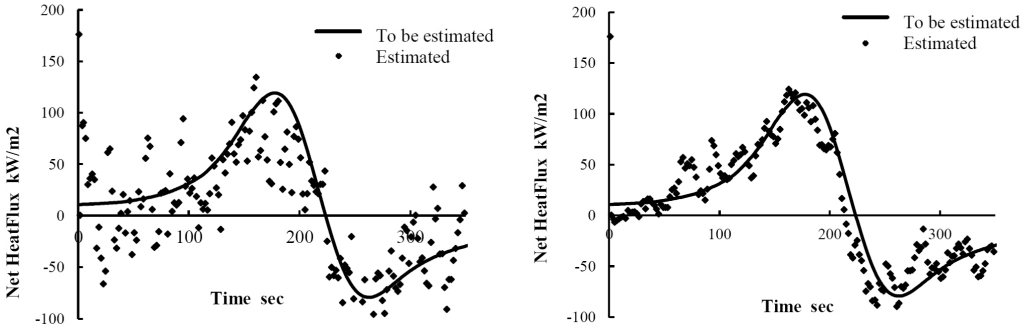

(a) $N_F = 10$ (b) $N_F = 20$

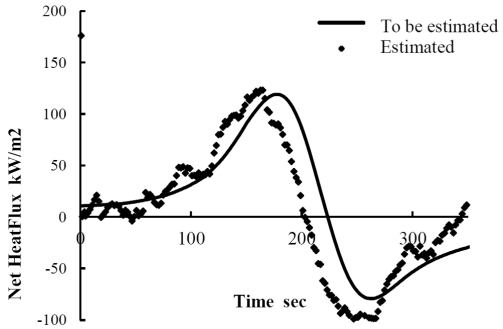

(c) $N_F = 30$

Figure 10: Result at C with Sequential Function Specification